Modeling of the non-uniform distributed GaN QDs based Infrared Photodetector

H. Fazlalipour [1], A. Asgari [2,3,*], G. Darvish [1]

1. Department of Electrical Engineering, Science and Research Branch, Islamic Azad University, Tehran 14778-93855, Iran
2. Research Institute for Applied Physics and Astronomy, University of Tabriz, Tabriz 55165-163, Iran
3. School of Electrical, Electronic and Computer Engineering, The University of Western Australia, Crawley, WA 6009, Australia
Email addresses: h_fazlalipour@srbiau.ac.ir, darvish_gh@srbiau.ac.ir
*Corresponding author: e-mail asgari@tabrizu.ac.ir , Phone: +98 41 3339 3005, Fax: +98 41 3334 7050

Received: 2020-11-16
Revised: 2021-02-11
Accepted: 2021-03-10

Abstract
In this paper, pyramidal shaped GaN-based quantum dots (QDs) with different sizes in each layer, surrounded by $Al_{0.2}Ga_{0.8}N$ is proposed for infrared photodetector mainly to enhance the detector performance. In this model, we are considering the QDs sizes' distribution to calculate all parameters instead of using Poisson distribution to express the inhomogeneous broadening just in the absorption coefficient. To model the performance of the devices, the Schrödinger equation has been solved using the effective mass approximation; then, the absorption coefficient, the gain, the responsivity, the electron mobility, the dark current, and the detectivity as a function of temperature for different biases are obtained. Significant improvements in the optical behavior are seen in the modeled results at T = 220 K.

Keywords
Pyramidal quantum dots, infrared photodetector, non- uniform, temperature.

1. Introduction

Nitride based semiconductors are commonly important material for optical sources and detectors in the near-infrared, visible, and ultraviolet regions. Research efforts at nitride materials are mostly concentrated on understanding and controlling their optical properties. These properties are strongly affected by the existence of internal electric fields in the range of MV⁄cm [1-5]. These semiconductors with a wurtzite crystal structure are direct energy bandgap semiconductors and have many unparalleled features including wide bandgaps, high absorption, high-saturation velocity, and radiation coefficients, and stronger excitonic effects [6-10]. The QDs based on these materials can be used to produce and detect electromagnetic waves from infrared to ultraviolet frequency, by varying the dot size and composition. To improve the performance of these photodetectors, various structures with different materials have been investigated until now[11, 12]. The use of nitride quantum dots in the active area of optical components leads to higher temperature operations. The use of these materials of QDs makes the optical response almost insensitive to the displacement density. As an example of these nanostructures, the single-photon emission in a GaN-based quantum dot structure at a temperature of 200 K can be controlled by a cooling system, while it is possible in a material such as InAs at much lower temperatures [13, 14]. Nitride-based quantum dots can be generated by a variety of growth techniques such as molecular beam epitaxy (MBE) and metal-organic chemical vapor deposition (MOCVD) and other less developed methods, such as the solid-liquid-gas mechanism, and the likes. The self-assembled method using the Stranski–Krastanow growth is a good technique to fabricate QDs which results in the formation of pyramidal QDs [15]. The significant characteristics of these structures are reduced electron-phonon scattering, the ability to operate at high temperatures, and high current gain [16-18]. Recently, many studies have been done on Wurtzite III-nitride QDs for their potential use [19, 20]. However, the modeling and characterization of this kind of detectors are in the preliminary stage and need more attention. Here we proposed a pyramidal shape GaN QDs with different sizes in each layer, which is achieved experimentally by Stranski–Krastanow growth method. Given the quantum dot fluctuation in this growth method, we first calculated the Eigenfunctions, Eigenvalues, and other physical parameters for QDs in each layer. Then, the photodetector parameters such as absorption coefficient for different combinations of quantum dot sizes, gain and dark current as a function of temperature, responsivity as a function of wavelength and temperature, and temperature dependence detectivity in different bias were evaluated precisely.

2. Models

A schematic view of our modeled Quantum dot infrared photodetector (QDIP) structure (see Fig. 1), where GaN QDs are sandwiched between AlGaN barriers. As a case study, the total number of the quantum dot layers is 10, and QD density $N_d = 10^{24}\ m^{-3}$ is used as the active region of the device.

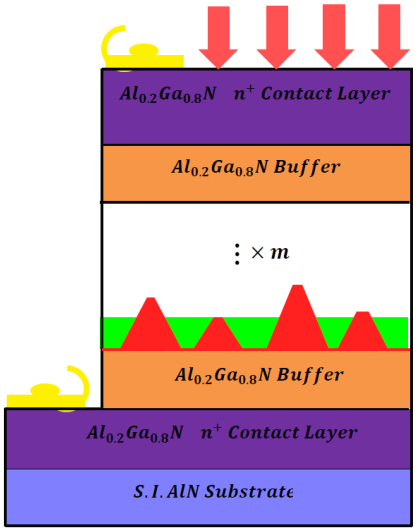

Fig. 1. A schematic view of the QDIP structure where the pyramids represent quantum dots.

The schematic representation of the theoretical configuration used in the calculations (see Fig. 2), in which a pyramidal shape GaN dots, which has been surrounded by $Al_{0.2}Ga_{0.8}N$, has been considered as a unit cell.

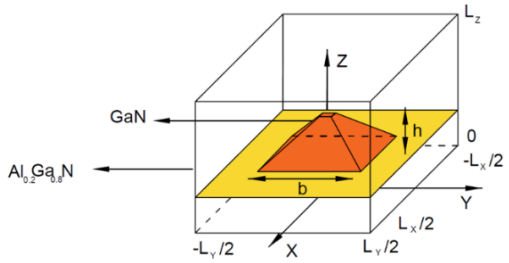

Fig. 2. A simple schematic diagram of pyramidal QD.

Since in the detector to collect the stimulated and excited carriers from the quantum dots, the device is always biased, and on the other hand, considering the properties of nitride materials that have a significant internal field, the Hamiltonian of the QD can be followed by (1).

$$H = \frac{-\hbar^2}{2}\nabla\frac{1}{m^*(x.y.z)}\nabla + V(x.y.z) + e\vec{F}\cdot\vec{r} \qquad (1)$$

where m^* is the electron effective mass, and $V(x.y.z)$ is given by (2):

$$V(x.y.z) = \begin{cases} 0 & inside\ QD \\ \Delta E_c & else \end{cases} \qquad (2)$$

where ΔE_c is the conduction band discontinuity[21] that can be followed by (3).

$$\Delta E_C = 0.7 \times \left(E_{g(Al_xGa_{1-xN})} - E_{g(GaN)}\right) \qquad (3)$$

'x' is an Al mole fraction in the barrier, and $\vec{F}$ refers to both the external and built-in electric fields.

The built-in electric field is given by (4) [22].

$$F_d = \frac{b(P_{tot}^{br} - P_{tot}^{d})}{\varepsilon_0(h\varepsilon_{br} + b\ \varepsilon_d)} \qquad (4)$$

where 'b' , and 'h' are the width of $Al_{0.2}Ga_{0.8}N$ barrier and height of GaN dot, respectively (as shown in Fig. 2). P_{tot}^{br}, and P_{tot}^{d} are total polarization; and ε_{br} , ε_d is the relative dielectric constant respectively for $Al_{0.2}Ga_{0.8}N$ barrier and GaN dot.

To express the electronic structure of the quantum dots, the easiest method is the wave expansion method using the effective mass approximation. This method, which has a high degree of accuracy, has also been studied by many authors [14, 21, 23-25].

In the pyramid QD, one can use a large rectangular cube box to capture the pyramidal dot and then develops QD wave functions based on sinusoidal and cosine wavefunctions of the unit cell. If the dimension of the unit cell is considered to be $\left[\frac{-L_x}{2}.\frac{L_x}{2}\right]$. $\left[\frac{-L_y}{2}.\frac{L_y}{2}\right]$. $[0.L_z]$ the wavefunction[26] that can be followed by (5).

$$\Psi(x.y.z) = \sum_{lmn} a_{lmn}\varphi_{lmn}(x.y.z) \qquad (5)$$

where $\varphi_{lmn}(x.y.z)$ expressed by "(see (6))".

$L_x.L_y.and\ L_z$ are lengths of the unit cell along the x, y and z directions, respectively.

The advantage of the normalized plane wave approach is the fact that there is no need to explicitly match the wave function, across the boundary of the barrier and quantum dot [26]. Therefore, using this method is suitable for an arbitrary confining potential. Using 17 normalized plane waves in each direction to achieve the convergence of the electron energy eigenvalues to less than 1 meV, a 4913×4913 matrix is formed.

Using the obtained wavefunctions, we can calculate the transition matrix element, which is one of the most significant agents that controls the absorption coefficient and oscillator strength. It is given by (7).

$$f_{eg} = \frac{2m^*}{\hbar^2}\left(E_e - E_g\right)\left|x_{eg}\right|^2 \qquad (7)$$

where x_{eg} is the in-plane x-transition matrix element from a ground state 'g' to an excited state 'e' with energy difference $\Delta E = \left(E_e - E_g\right) = \hbar\omega_{eg}$.

The absorption coefficient $\alpha(\omega)$ can be expressed by "(see (8))" [12].

$$\varphi_{lmn} = \sqrt{\frac{2}{L_x}} sin\left[l\pi\left(\frac{1}{2} - \frac{x}{L_x}\right)\right]\sqrt{\frac{2}{L_y}} sin\left[m\pi\left(\frac{1}{2} - \frac{y}{L_y}\right)\right]\sqrt{\frac{2}{L_z}} sin\left[n\pi\left(\frac{z}{L_z}\right)\right] \quad (6)$$

$$\alpha = \frac{\pi\hbar N_d n_{op} e^2}{m^* \varepsilon\varepsilon_0 c}\left\{\frac{\Gamma}{\left(\hbar\omega - \hbar\omega_{eg}\right)^2 + \Gamma^2}\right\}(n_g - n_e) f_{eg} \quad (8)$$

where N_d is the number of dots per unit volume, n_{op} its refractive index, c is the velocity of light, ε_0 and ε is the permeability of free space and the medium, respectively. The lifetime broadening is Γ, n_g . and n_e are occupation probabilities of the ground and excited states, respectively.

As mentioned before, we investigate a more realistic structure assuming pyramidal shape GaN QDs with different sizes in each layer, which achievable experimentally by Stranski–Krastanow growth method. Therefore, we assumed different QDs, and the size of the QDs is shown in Table I. Using the QDs given in Table I, we have assumed three different series with a combination of different percentages of QDs in a layer to make the active region. The series is given in Table II.

Table I. The different size of QD.

QD Types	Quantum dot size $(nm \times nm \times nm)$
Dot 1	$6 \times 6 \times 3$
Dot 2	$7 \times 7 \times 3$
Dot 3	$8 \times 8 \times 3$
Dot 4	$8 \times 8 \times 4$
Dot 5	$9 \times 9 \times 4$
Dot 6	$10 \times 10 \times 4$
Dot 7	$10 \times 10 \times 5$

Table II. The different combinations of QDs are used for simulations.

QD series	Sorting Dots(%)						
	Dot 1	Dot 2	Dot 3	Dot 4	Dot 5	Dot 6	Dot 7
Series A	4	9	17	40	17	9	4
Series B	2	4	14	60	14	4	2
Series C	1	2	7	80	7	2	1

Besides, to determine the built-in electric fields in this structure and to include it in solving the Hamiltonian equation, the parameters are given by "(see Table III)".

Fig. 3 is showing the absorption coefficient for series A, B, and C. The black- lines show the absorption coefficient for each QDs in the layer and the red-lines show the absorption coefficients for the series. As can be seen from Fig. 3, by increasing the uniformity of QDs in the layers (increasing the ratio of the QDs-4 and decreasing other QDs percentages), the peak of the absorption coefficient increases but its width decreases.

The comparison of the absorption coefficient's main peak for each series is given in Table IV.

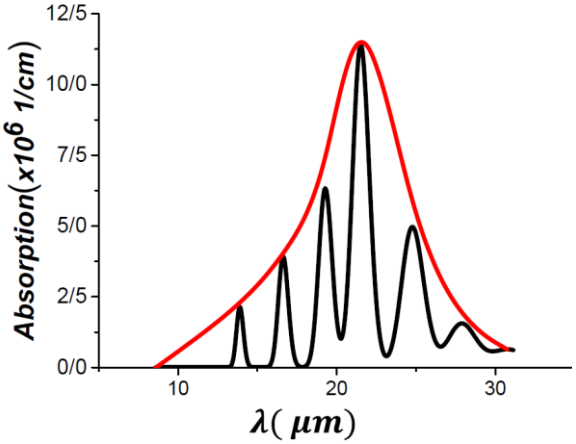

(a)

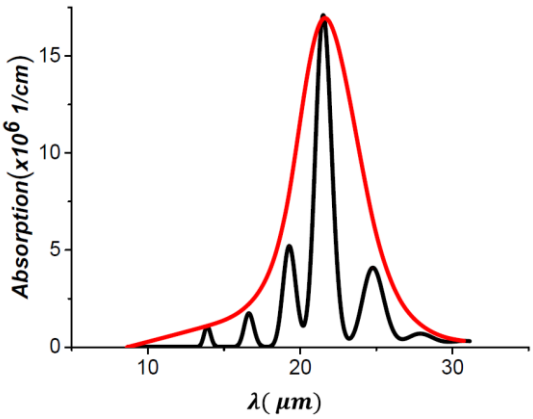

(b)

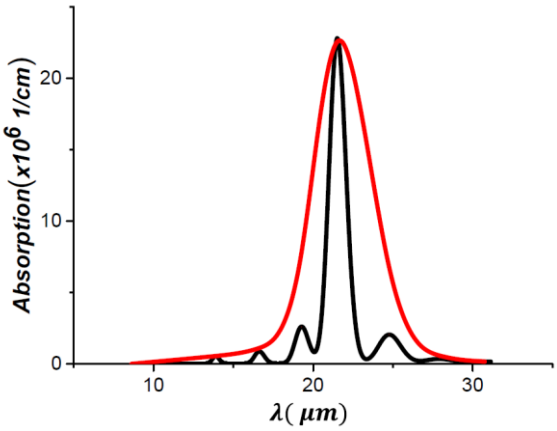

(c)

Fig. 3. Absorption coefficient of $Al_{0.2}Ga_{0.8}N/GaN$. (a) Series A, (b) Series B, (c) Series C.

Table III. Lattice constant, dielectric and elastic constants, spontaneous and piezoelectric polarization for GaN, AlN, and $Al_xGa_{1-x}N$ used to calculate the built-in electric fields [27].

Wurtzite, selected physical constants	GaN	AlN	$Al_xGa_{1-x}N$
$a(A)$	3.189	3.112	$-0.077x + 3.189$
$e_{31}(C/m^2)$	-0.49	-0.60	$-0.11x - 0.49$
$e_{33}(C/m^2)$	0.73	1.46	$0.73x + 0.73$
$c_{13}(GPa)$	103	108	$5x + 103$
$c_{33}(GPa)$	405	373	$-32x + 405$
ε	10.4	10.1	$0.3x + 10.4$
$P_{SP}(C/m^2)$	-0.029	-0.081	$-0.052x - 0.029$
$P_{piezo}(C/m^2)$	-0.0066	-	-

Table. IV. The comparison of the main peak for the QD series.

QD series	The main peak of absorb ($\times 10^6$ 1/cm)
Series A	11.4
Series B	17.1
Series C	22.8

3. Result and discussion

3.1. Photoconductive gain

The photoconductive gain in QDIPs is expressed in terms of the capture probability p_c by (9) [15].

$$g_p = \frac{1 - p_c}{Kp_cF} \tag{9}$$

where $p_c \ll 1$, K is the number of quantum dot layers and F is the fill factor for a single layer. p_c can also be defined as $p_c = \frac{\tau_{trans}}{\tau_{life}}$, where τ_{trans} is the transit time and can be calculated by (10).

$$\tau_{trans} = \frac{h}{\mu F}\sqrt{1 + \left(\frac{\mu F}{v_s}\right)^2} \tag{10}$$

and τ_{life} is the recombination time (lifetime) and expresses by (11) [25].

$$\tau_{life} = \frac{(K+1)L}{\pi a_{QD}^2 h \sum_{QD} V_t} \tag{11}$$

Then

$$p_c = \frac{\pi a_{QD}^2 h^2 \sum_{QD} V_t \sqrt{1 + \left(\frac{\mu F}{v_s}\right)^2}}{(K+1)L\mu F} \tag{12}$$

where a_{QD} the lateral size of quantum dots, V_t the capture rate of electrons, $\sum_{QD}$ is the quantum dot density in each quantum dot layer, v_s is saturation velocity of the electron, L is the distance between quantum dot layers, F is the bias voltage that allows to minimize the capture probability and improve the photoconductive gain of QDIP, and μ is the mobility of electron for $Al_{0.2}Ga_{0.8}N/GaN$ structure.

To calculate mobility, we have used different scattering mechanisms as reported by Asgari *et.al.* [28].

The calculated electron mobility as a function of temperature for $Al_{0.2}Ga_{0.8}N/GaN$ structure (see Fig. 4).

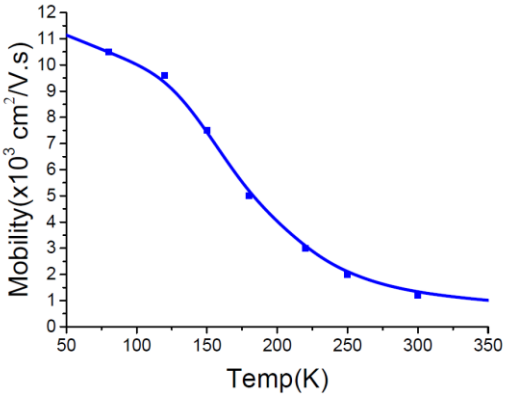

Fig. 4. The mobility of electron for $Al_{0.2}Ga_{0.8}N/GaN$ as a function of temperatures.

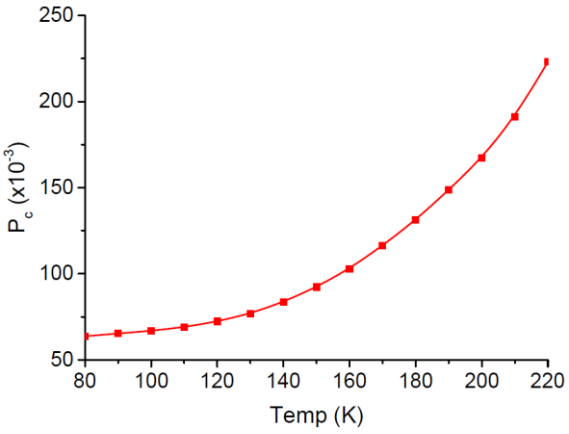

(a)

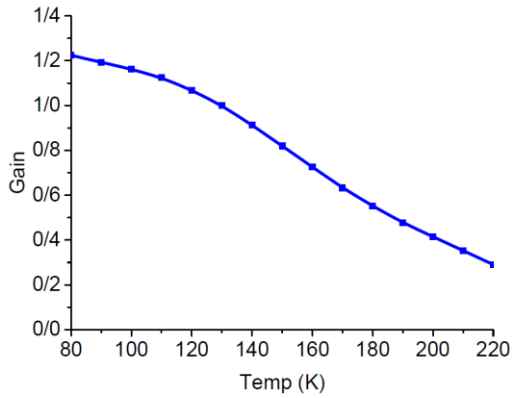

(b)

Fig. 5. (a) The capture probability, (b) The gain of $Al_{0.2}Ga_{0.8}N/GaN$ QDs.

The infrared photodetector performance is determined approximately by the capture probability of the QDs and the photo-generation rate of carriers out of the QDs. The capture probability determines the responsivity through the photoconductive gain. The gain and electron capture probability can thus be calculated using (9) and (12). Fig .5 shows the capture probability and photoconductive gain as a function of temperature for the proposed QDIP.

As shown in Fig. 5a, the capture probability (p_c) increases with increasing temperature. Although the whole number of states remains constant due to the thermal emission, the number of unoccupied electron states in the QDs increases with temperature, and hence the p_c increases with an amount proportional to $e^{\frac{E_i}{k_B T}}$.

Since capture probability and as a result, the gain is expressed in terms of material and structural parameters in (12) and (9), it is possible to optimize the photodetector for higher gain. Hence, the material with high mobility, a large number of QDs layers with optimized total thickness, the thickness of the barrier is some of the parameters that improve photodetectors' performance.

3.2. Responsivity

Responsivity is one of the most important parameters of QDIP and is defined as the ratio of its output electrical signal to the input optical signal. It is given by (13).

$$R = \frac{e}{\hbar\omega} g_p \eta \tag{13}$$

Where η is the quantum efficiency that can be calculated by (14).

$$\eta(\hbar\omega) = 1 - exp\left(-\alpha(\hbar\omega) \cdot l_{eff}\right) \tag{14}$$

where $\alpha(\hbar\omega)$ is the absorption coefficient and l_{eff} is the effective length of the absorption region.

By knowing the absorption coefficient and gain, the responsivity can be introduced for each series of QDs in terms of wavelength and temperature as shown in Fig. 6.

As shown in Fig. 6, concerning (9), with increasing temperature, the gain decreases, and as a result, the responsivity decreases. A further increase in temperature will result in a decrease in the absorption coefficient and, consequently, will reduce quantum efficiency, which results in reduced responsivity. In other words, with the temperature rise continuing, the number of electrons in the QDs will increase due to the dark current, which will result in a reduction in the number of stimulated emptying levels, thus reducing the optical response of the detector.

3.3. Dark current

In QD photodetectors, in the absence of light, there is a current in the device, which is the dark current. This unwanted current is due to factors such as thermionic emission, field-induced emission, and ground-state sequential tunneling. The dark current density can be given by (15) [29].

$$J_{dark} = ev_D n_{3D} \tag{15}$$

Where v_D is the drift velocity and n_{3D} is the electron density, which can be given by (16) [29].

It is known that the temperature dependence of the dark current under a certain electric field behaves exponentially. In Fig. 7, the influence of temperature on the dark current for the fixed electric field, Bias = 0.6 V, is displayed. It is known that the shape of the curve is increasing with temperature increases, which can be due to electrons escaping from the quantum dot by the thermionic emission. It should be mentioned that GaN self-assembled QDIP has a very low dark current in comparison to the structure introduced in Ref [30].

$$n_{3D} = 2\left(\frac{m_b k_B T}{2\pi\hbar^2}\right)^{3/2} exp\left(-\frac{E_a}{kT}\right) \tag{16}$$

Where k_B is the Boltzmann constant, m_b is the electron effective mass in the barrier, and E_a is the activation energy which is equal to the sum of the energy difference between the Fermi level and the top of conduction band edge and the ionization energy of the quantum dots.

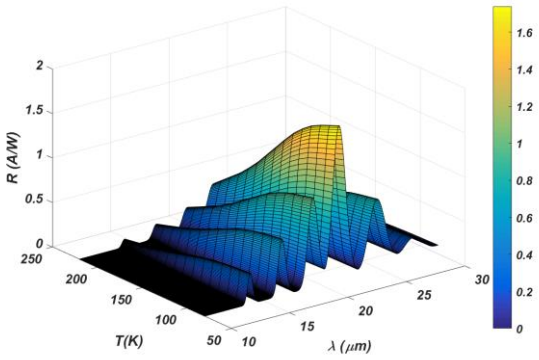

(a)

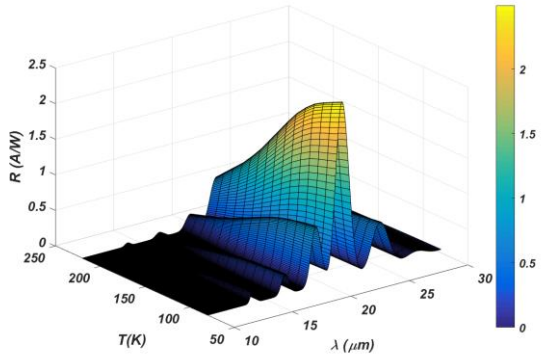

(b)

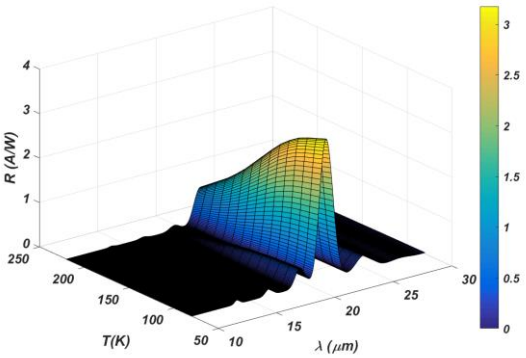

(c)

Fig. 6. The responsivity of $Al_{0.2}Ga_{0.8}N/GaN$ QDIP. (a) series A, (b) series B, (c) series C.

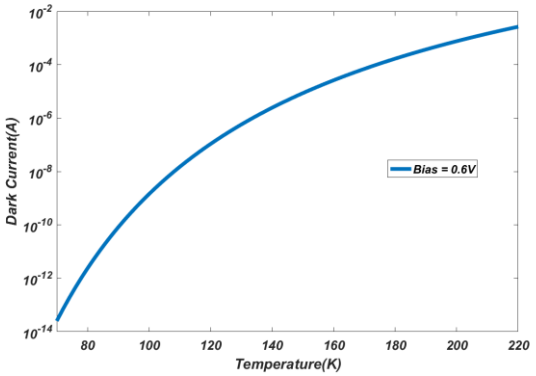

Fig. 7. Dark current as a function of temperature at Bias = 0.6 V.

3.4. *Detectivity*

Detectivity is one of the most important factors of a detector. This quantity determines how small the incoming light can be detected, and is a quantity for signal-to-noise measurements. The normalized detectivity of QDIP is defined by (17) [25].

$$D^* = \frac{\eta}{2h\upsilon}\sqrt{\frac{eg_n}{J_{dark}}} \tag{17}$$

where g_n is the noise gain and equals the photoconductive gain $g_n = g_p$.

Fig. 8, shows the dependence of the detectivity on temperature plotted for various biases. Moreover, it shows the detectivity decreases with the increase of the temperature at certain bias, for example, at the $bias = 0.8\,V$, when the temperature increases from $77^{\circ}K$ to $220^{\circ}K$, corresponding detectivity rapidly decrease from5.13×10^8 to 1.31×10^8 $cm\sqrt{Hz}/W$, respectively.

The reasons for the decrease in detectivity are as follows: as the temperature rises, the thermal emission increases, so that more electrons can easily leave the quantum dot to form the dark current and the noise, which eventually leads to the decrease in detectivity. Finally, since the internal electric field in nitride materials is strong, so electric field changes do not have much effect on the detectivity.

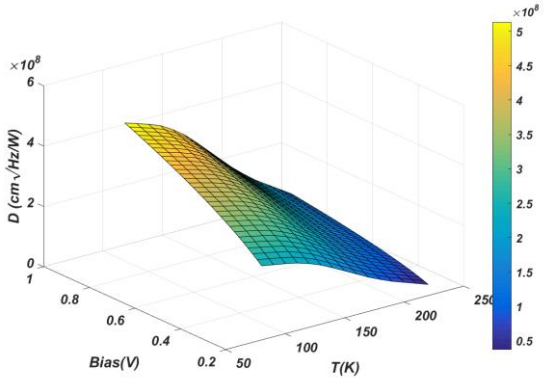

Fig. 8. Detectivity (at $\lambda = 21.5\,\mu m$) as a function of temperature for various bias for series C.

4. Conclusion

We modeled the inferred photodetectors based on GaN QDs with different QDs sizes in a layer, as self-assembled QDs. In the calculation, using three different series of QDs, with solving Schrodinger equation and taking into the effects of temperatures and bias, the properties such as electron mobility, noise, dark current, responsivity, and detectivity are obtained. The proposed structure benefited from high detectivity and improved optical characteristics such as absorption coefficient and dark current. The results show that more uniform QDs in the layer results in higher absorption than higher responsivity. Besides, the obtained amount for dark current and the detectivity at T = 220 K, promise the use of these detectors without the need for a cooling system.

5. References

[1] T. Ashley, T. Burke, G. Pryce, A. Adams, A. Andreev, B. Murdin, E. O'Reilly, C. Pidgeon, "InSb 1− x N x growth and devices", *Solid-State Electronics*, vol. 47, no. 3, pp. 387-394, 2003.

[2] D. Huang, M.A. Reshchikov, H. Morkoç, "Growth, structures, and optical properties of III-nitride quantum dots", *International journal of high-speed electronics and systems*, vol. 12, no. 01, pp. 79-110, 2002.

[3] M. Dworzak, T. Bartel, M. Straßburg, I. Krestnikov, A. Hoffmann, R. Seguin, S. Rodt, A. Strittmatter, D. Bimberg, "Optical properties of InGaN quantum dots", *Superlattices and Microstructures*, vol. 36, no. 4-6, pp. 763-772, 2004.

[4] B. Monemar, P. Paskov, A. Kasic, "Optical properties of InN—the bandgap question", *Superlattices and Microstructures,* vol. 38, no. 1, pp. 38-56, 2005.
[5] T. Matsuoka, "Progress in nitride semiconductors from GaN to InN-MOVPE growth and characteristics", *Superlattices and Microstructures,* vol. 37, no. 1, pp. 19-32, 2005.
[6] M. Mexis, S. Sergent, T. Guillet, C. Brimont, T. Bretagnon, B. Gil, F. Semond, M. Leroux, D. Néel, S. David, "High quality factor nitride-based optical cavities: microdisks with embedded GaN/Al (Ga) N quantum dots", *Optics letters,* vol. 36, no. 12, pp. 2203-2205, 2011.
[7] D. Williams, A. Andreev, E. O'Reilly, "Dependence of exciton energy on dot size in Ga N⁄Al N quantum dots", *Physical Review B,* vol. 73, no. 24, pp. 241301, 2006.
[8] V. Domen, "GaN-based blue laser diodes grown on SiC substrate as light source of high-density optical data storage", *Fujitsu Sci. Tech. J,* vol. 34, no. 2, pp. 191-203, 1998.
[9] A. Asgari, E. Ahmadi, M. Kalafi, "AlxGa 1− xN/GaN multi-quantum-well ultraviolet detector based on pin heterostructures", *Microelectronics Journal,* vol. 40, no. 1, pp. 104-107, 2009.
[10] A. Asgari, L. Faraone, "SiN passivation layer effects on un-gated two-dimensional electron gas density in AlGaN/AlN/GaN field-effect transistors", *Applied Physics Letters,* vol. 100, no. 12, pp. 122106, 2012.
[11] S. Wang, M. Lo, H. Hsiao, H. Ling, C. Lee, "Temperature dependent responsivity of quantum dot infrared photodetectors", *Infrared physics & technology,* vol. 50, no. 2, pp. 166-170, 2007.
[12] H. Lim, W. Zhang, S. Tsao, T. Sills, J. Szafraniec, K. Mi, B. Movaghar, M. Razeghi, "Quantum dot infrared photodetectors: comparison of experiment and theory", *Physical Review B,* vol. 72, no. 8, pp. 085332, 2005.
[13] S. Kako, C. Santori, K. Hoshino, S. Götzinger, Y. Yamamoto, Y. Arakawa, "A gallium nitride single-photon source operating at 200 K", *Nature materials,* vol. 5, no. 11, pp. 887, 2006.
[14] A. Gueddim, T. Eloud, N. Messikine, N. Bouarissa, "Energy levels and optical properties of GaN spherical quantum dots", *Superlattices and Microstructures,* vol. 77, pp. 124-133, 2015.
[15] J. Phillips, P. Bhattacharya, S. Kennerly, D. Beekman, M. Dutta, "Self-assembled InAs-GaAs quantum-dot intersubband detectors", *IEEE Journal of Quantum Electronics,* vol. 35, no. 6, pp. 936-943, 1999.
[16] D. Pan, E. Towe, "Conduction intersubband (In, Ga) As/GaAs quantum dot infrared photodetectors", *Electronics Letters,* vol. 34, no. 19, pp. 1883-1884, 1998.
[17] L. Jiang, S. Li, N. Yeh, J. Chyi, C. Ross, K. Jones, "In 0.6 Ga 0.4 As/GaAs quantum-dot infrared photodetector with operating temperature up to 260 K", *Applied physics letters,* vol. 82, no. 12, pp. 1986-1988, 2003.
[18] Z. Ye, J.C. Campbell, Z. Chen, E. Kim, A. Madhukar, "Noise and photoconductive gain in InAs quantum-dot infrared photodetectors", *Applied physics letters,* vol. 83, no. 6, pp. 1234-1236, 2003.
[19] N. Suzuki, N. Iizuka, K. Kaneko, "Simulation of ultrafast GaN/AlN intersubband optical switches", *IEICE transactions on electronics,* vol. 88, no. 3, pp. 342-348, 2005.
[20] S.H. Park, W.P. Hong, J. Kim, "Confinement-dependent exciton binding energy in wurtzite GaN/AlxIn1− xN quantum dots", *Superlattices and Microstructures,* vol. 109, pp. 254-258, 2017.
[21] A. Asgari, S. Razi, "High performances III-Nitride quantum dot infrared photodetector operating at room temperature", *Optics express,* vol. 18, no. 14, pp. 14604-14615, 2010.
[22] S. De Rinaldis, I. D'Amico, E. Biolatti, R. Rinaldi, R. Cingolani, F. Rossi, "Intrinsic exciton-exciton coupling in GaN-based quantum dots: Application to solid-state quantum computing", *Physical Review B,* vol. 65, no. 8, pp. 081309, 2002.
[23] J. Phillips, P. Bhattacharya, S. Kennerly, D. Beekman, M. Dutta, "Self-assembled InAs-GaAs quantum-dot intersubband detectors", *IEEE Journal of Quantum Electronics,* vol. 35, no. 6, pp. 936-943, 1999.
[24] M. Zavvari, V. Ahmadi, A. Mir, "High performance avalanche quantum dot photodetector for mid-infrared detection", *Optical and Quantum Electronics,* vol. 47, no. 5, pp. 1207-1217, 2014.
[25] H. Fazlalipour, A. Asgari, G. Darvish, "Modeling of pyramidal shape quantum dot infrared photodetector: the effects of temperature and quantum dot size", *Journal of Nanophotonics,* vol. 12, no. 2, pp. 026006, 2018.
[26] M. Califano, P. Harrison, "Presentation and experimental validation of a single-band, constant-potential model for self-assembled InAs/GaAs quantum dots", *Physical Review B,* vol. 61, no. 16, pp. 10959, 2000.
[27] F. Bernardini, V. Fiorentini, "Spontaneous versus piezoelectric polarization in III–V nitrides: conceptual aspects and practical consequences", *physica status solidi (b),* vol. 216, no. 1, pp. 391-398, 1999.
[28] A. Asgari, M. Kalafi, L. Faraone, "Effects of partially occupied sub-bands on two-dimensional electron mobility in Al x Ga 1− x N/GaN heterostructures", *Journal of applied physics,* vol. 95, no. 3, pp. 1185-1190, 2004.
[29] H. Liu, "Quantum dot infrared photodetector", *Optoelectronics Review,* no. 1, pp. 1-6, 2003.
[30] Z. Ye, J. C. Campbell, Z. Chen, E.T. Kim, A. Madhukar, "Normal-incidence InAs self-assembled quantum-dot infrared photodetectors with a high detectivity", *IEEE journal of quantum electronics,* vol. 38, no. 9, pp. 1234-1237, 2002.